

Flexoelectricity in WS₂

Measuring Electromechanical Coupling with Piezoresponse
Force Microscopy

Kalhan Koul

A thesis presented for Honor's Distinction



Department of Electrical and Computer Engineering

University of Texas at Austin

Fall 2018

Dedication

To my parents, for helping me find my passion for education and research.

Acknowledgements

First, I would like to thank my thesis advisor, Professor Edward Yu, for his guidance, support, and instruction. Over the last three years, Professor Yu's mentorship has helped me become a better student, researcher, writer, and engineer. As I move on to graduate school, I look forward to employing the habits and lessons I learned from him. I would also like to thank Professor Emanuel Tutuc for providing ideas and support for my thesis and Professors Jacob Abraham and Lizy John for guidance and help during the graduate school application process. Additionally, I would like to thank Dr. Chris Brennan. Three years ago, Chris, a graduate student at the time, seamlessly incorporated me into current projects, taught me about the research process, and was a great role model for me. My sophomore year I had little to no understanding of the ongoing projects, but Chris found a way to make me feel involved and useful and for that I am grateful. Finally, I would like to thank the Electrical and Computer Engineering Department and the Plan II Department for giving me the opportunity to write this thesis.

Abstract

Electromechanical coupling is the connection between mechanical properties, such as strain and strain gradients, and electronic properties, such as dielectric polarization fields. In piezoelectricity, the best known example of this effect, polarization is due to uniform strain. However, in flexoelectricity, a property that has been much less extensively explained, polarization is due to a strain gradient. Understanding flexoelectricity has applications in energy harvesting, biotechnology, and wearable devices. However, few papers discuss the property and it is not well understood. Monolayer MoS₂, a transition metal dichalcogenide (TMD), has recently been shown to produce an out-of-plane electromechanical response in atomically thin layers, which is evidence of flexoelectricity. In this thesis, the flexoelectric properties of WS₂, another TMD, is examined. Using piezoresponse force microscopy combined with a background subtraction method, one can show the presence of out-of-plane electromechanical coupling. This thesis will show that out-of-plane electromechanical coupling exists for WS₂, and that this is evidence of flexoelectricity.

Contents

1	Introduction	8
1.1	Motivation	8
1.1.1	Understanding Flexoelectricity	9
1.1.2	Applications in Electronics	10
1.2	Thesis Overview	11
1.2.1	Chapter Descriptions	11
1.2.2	Contributions	13
2	Theory	14
2.1	Electromechanical Coupling	14
2.1.1	Strain, Polarization Fields, and Piezoelectricity	15
2.1.2	Centrosymmetry	17
2.1.3	Strain Gradients	18
2.2	Flexoelectricity	19
2.2.1	Direct and Converse Effect	20
2.2.2	Why Monolayer WS ₂ ?	21

2.2.3	Piezoresponse Force Microscopy	23
2.2.4	Kogan's Estimate	24
2.2.5	Summary	25
3	Methods	26
3.1	Sample Preparation	26
3.1.1	Cleaning the Substrate	26
3.1.2	Mechanical Exfoliation	27
3.2	Characterizing Monolayer WS ₂	29
3.2.1	Raman Spectroscopy	29
3.2.2	Photoluminescence	31
3.3	Atomic Force Microscopy	32
3.4	Piezoresponse Force Microscopy	35
4	Experimental Results	38
4.1	Characterizing Monolayer WS ₂	38
4.1.1	Raman Spectroscopy	39
4.1.2	Photoluminescence	42
4.2	Atomic Force Microscopy	43
4.3	Piezoresponse Force Microscopy	48
4.4	Background Subtraction Method	51
4.5	Calculating d ₃₃ ^{eff}	52
4.6	Summary of Results	54

5 Conclusion	56
5.1 Understanding the Results and Limitations of the Experiment	56
5.2 Comparison to Kogan’s Estimate	58
5.3 Summary of Research and Future Work	60

Chapter 1

Introduction

1.1 Motivation

Understanding the coupling between mechanical and electronic properties in 2D materials can lead to a variety of potential engineering applications including applications in biotechnology such as wearable devices, energy harvesters, sensors, and actuators. Piezoelectricity, which connects uniform strain with dielectric polarization, was first predicted theoretically in certain 2D materials in 2012 [1] and was subsequently confirmed experimentally [2]. On the other hand, flexoelectricity, the relationship between strain gradients and polarization, is a form of this coupling whose investigation is still in its early stages. Studying flexoelectricity will not only help further the understanding of electromechanical coupling, but also lead to a better understanding of its potential applications.

1.1.1 Understanding Flexoelectricity

Although flexoelectricity was initially discovered over fifty years ago, it has not been studied extensively due to its small magnitude in bulk materials[3]. Now that the technology exists to create atomically thin layers, studying flexoelectricity experimentally is viable, since the flexoelectric effect can be of much greater magnitude. Simply stated, flexoelectricity can be understood as polarization due to a strain gradient [4]. Strain gradients are much easier to create in nanomaterials, since a strain over a smaller distance creates a larger gradient. This allows flexoelectricity to have a greater affect in thin materials. Therefore, transition metal dichalcogenides (TMDs) are particularly attractive, because they are composed of monolayers, or single atomic layers, bound together by Van der Waals forces. Layers of these materials can be pulled apart with much greater ease than other bulk materials, enabling atomically thin materials to be created. These layers are useful, because they do not have the same limitations on achievable strain gradients that bulk materials have.

Flexoelectricity can manifest in two distinct, but closely related ways: direct and converse. For the direct effect, a strain gradient causes a polarization. For the converse effect, an electric field gradient creates a strain in the material[3]. These effects and their respective mathematical descriptions will be further discussed in Chapter 2 of this thesis. In the work performed for this thesis, the converse effect is studied using piezoresponse force microscopy. Studying the converse effect will further the understanding of electromechan-

ical coupling and therefore, allow for technological development.

Understanding flexoelectricity is important for multiple reasons. One reason is that flexoelectricity occurs in all materials, unlike piezoelectricity [5]. Piezoelectricity occurs only in noncentrosymmetric materials, which lack a center of inversion symmetry. However, since a nonuniform strain removes inversion symmetry, nonuniform strain can cause polarization [6]. A further explanation of inversion symmetry, and the crystallographic factors involved will be discussed in Chapter 2. Since it is not limited by symmetry, flexoelectricity is associated with a much broader range of materials. Additionally, since the small length scales characteristic of nanomaterials can lead to larger strain gradients, flexoelectricity can play a much bigger role in nanoscale devices than in macroscale devices. For these reasons, understanding flexoelectricity will open the door to novel applications.

1.1.2 Applications in Electronics

Understanding the relationship between electronic and mechanical properties in a material is essential for many applications in engineering including biotechnology, wearable devices, energy harvesters [7], sensors [8], and actuators[9]. Additionally, as previously discussed, studying flexoelectric coupling requires characterization on a small scale since large strain gradients can be introduced. A better understanding of flexoelectricity on the nanoscale will allow for new, smaller devices. Moore’s law is the observation that size of integrated circuits exponentially decrease over time. Following this trend,

the length at which structures can be engineered becomes smaller, and since flexoelectricity is most evident in nanotechnology, this presents an opportunity for engineering innovation. One example of an application is energy harvesting for small devices such as wearables. Utilizing piezoelectricity and flexoelectricity to generate energy would allow these devices to be powered more conveniently. Therefore, furthering the understanding of flexoelectricity in 2D materials will help create breakthroughs in engineering.

1.2 Thesis Overview

1.2.1 Chapter Descriptions

In Chapter 2, the theory behind flexoelectricity will be examined. First, the basics of electromechanical coupling, including how strain and polarization interact, are discussed. Then, piezoelectricity and homogenous strain are presented and explained. The morphological characteristics that enable piezoelectricity are detailed and flexoelectricity is introduced. Next, the difference between the direct and converse effects for both piezoelectricity and flexoelectricity are discussed and the technical details of piezoresponse force microscopy and other experimental procedures employed will be explained. This includes why WS₂ was chosen, a brief and high level explanation of the experiment, and an estimate of the flexoelectric coefficient using techniques from literature.

In Chapter 3, the experimental methods will be described in detail. First,

the process of preparing the sample, including cleaning the substrate and exfoliating the WS₂, will be discussed. Second, the process of determining whether or not a sample of WS₂ consists of a single monolayer is described. This includes characterizing the sample with both Raman spectroscopy and photoluminescence to see their respective signatures for different numbers of layers. Next, the process of atomic force microscopy (AFM) is explained. AFM is used to understand the topography of the sample. Finally, piezoresponse force microscopy is described in detail as it is the main method of gathering electromechanical information.

In Chapter 4, the experimental results will be presented and discussed. First, determining the number of layers is described in detail. This includes showing the Raman spectra and photoluminescence results and comparing them to the literature discussed in Chapter 3. After that, the AFM data will be presented and an analysis of the height information will help determine and confirm that monolayer material has been found. Finally, PFM results will be discussed and explained, and a description of the data analysis and the background subtraction method used to isolate the flexoelectric signal will be given.

In Chapter 5, the final results of the experiment are presented and the variation in the value for d^{eff} is discussed. To understand this variation, the possible limitations of the way this experiment implemented PFM are discussed. Then, the relevant equations for the final calculation of μ^{eff} are presented and the calculated μ^{eff} is compared to Kogan's estimate for flexo-

electricity in WS₂. Finally, a summary of the experiment and a discussion of future work is considered.

1.2.2 Contributions

This thesis will discuss the measurement of out-of-plane electromechanical effects in WS₂ and how these effects provide evidence for flexoelectricity. To accomplish this task, this thesis will discuss the specifics of characterizing monolayer WS₂, atomic force microscopy, piezoresponse force microscopy, and the calculations involved in measuring the effective flexoelectric constant, μ^{eff} . Finally, one can acknowledge that the measurement of an out-of-plane electromechanical effect provides a platform for new applications of electromechanical properties in sensors, actuators, and energy harvesters. Therefore, this thesis helps develop knowledge of flexoelectricity, characterizes the electromechanical effects of WS₂, and demonstrates possible avenues for novel applications.

Chapter 2

Theory

2.1 Electromechanical Coupling

Electromechanical coupling is the relationship between mechanical and certain electronic properties in a material. To understand flexoelectricity and the mechanism of electromechanical coupling, this section will first provide a discussion of strain and how it can cause a polarization field. Then, to build an understanding of flexoelectricity, piezoelectricity, the most-well understood electromechanical effect, is examined. After that, crystal structure and centrosymmetry, the fundamental characteristics that differentiate piezoelectricity and flexoelectricity, are discussed and flexoelectricity's advantages are highlighted.

2.1.1 Strain, Polarization Fields, and Piezoelectricity

To understand electromechanical coupling, it is useful to first develop a general understanding of how strain can create a dielectric polarization field. Strain is the reaction of a system to applied stress. Put differently, strain is the amount of deformation of a material in response to a given stress. Polarization fields are vector fields consisting of the induced electric dipole moments in a material. Normally, the dipole moments in a material are zero and there is no polarization field. However, under strain dipole moments can be created and a polarization field is induced. Figure 2.1 shows an example of the crystal quartz under stress in the vertical direction. Here, one can see the effects of both stretching and compressing the material, and how it can create polarization.

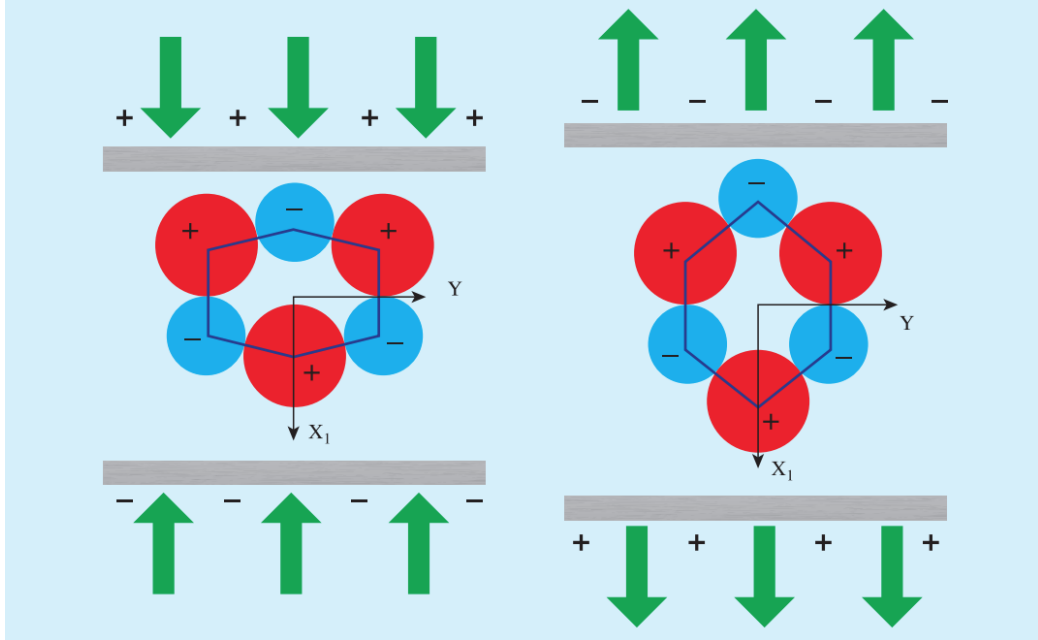


Figure 2.1: The left side of the figure shows compression causing polarization with positive charges on the top and negative charges on the bottom. The right side of the figure shows stretching causing polarization in the reverse direction. This figure shows how strain can cause polarization. [10]

When strain is homogenous and a polarization field is induced, the phenomenon is called the direct piezoelectric effect. On the other hand, when an electric field is applied to a material and it causes mechanical deformation, it is called the converse piezoelectric effect. The formulas for these two equations are given below.

$$P_i = d_{ijk}\sigma_{jk}$$

$$\varepsilon_{jk} = d_{ijk}E_i$$

P , E , d , σ , and ε , represent polarization, electric field, the piezoelectric coefficient, stress and strain, respectively. The subscripts i, j, and k represent the cartesian directions. The units of d are Coulombs per Newton (C/N), or equivalently, meters per Volt (m/V). For the direct effect, the piezoelectric coefficient can be thought of as the charge built up for the force applied (C/N). For the converse effect, the coefficient can be thought of as the displacement for an applied voltage (m/V). However, the piezoelectric effect does not occur in every material.

2.1.2 Centrosymmetry

The existence of piezoelectricity in a material is dependent on the material's crystal symmetry. Specifically, the material must be non-centrosymmetric for piezoelectricity to be present. A crystal is centrosymmetric when all points in the unit cell (x,y,z) are indistinguishable from (-x,-y,-z). This property is called inversion symmetry. Centrosymmetric materials under homogeneous strain still display centrosymmetric behavior; there is no polarization since the dipole moments are all still zero. Therefore, centrosymmetric materials show no piezoelectric activity[3]. However, in the presence of strain gradients, it is possible to undo the balancing effects of centrosymmetry and create polarization. The relationship between strain gradients and polarization is called flexoelectricity.

2.1.3 Strain Gradients

Varying strain at different points in a crystal creates an asymmetry in charge that allows polarization to occur. Since strain varies with position, dipole moments no longer balance each other even in centrosymmetric materials. Figure 2.2 shows the difference between homogenous strain and a strain gradient. For a centrosymmetric material under homogenous strain, there is no polarization because the center of positive and negative charge does not shift. However, for a centrosymmetric material under a strain gradient, asymmetry in the gradient allows polarization to occur.

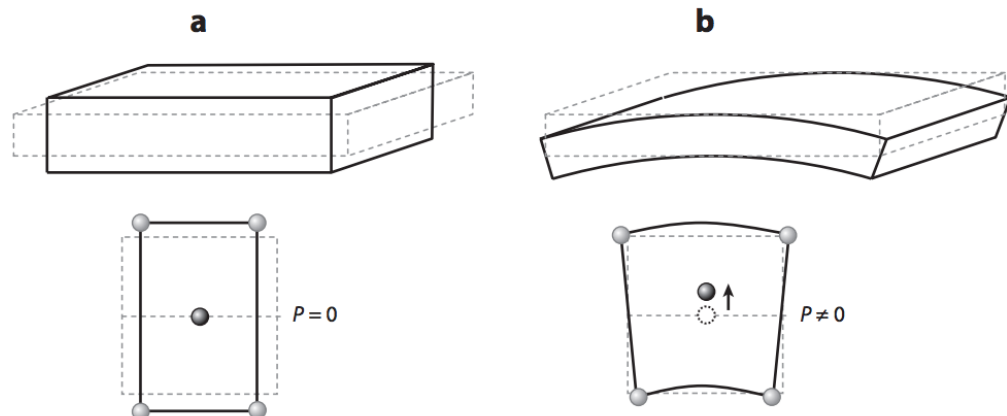


Figure 2.2: Side (a) shows centrosymmetric material under homogenous strain, which causes no polarization. Side (b) shows the same material under a strain gradient, which causes polarization. The shaded spheres in the bottom half of the figure represent the center of positive and negative charge. [3]

Therefore, a strain gradient can create polarization, independent of the

crystal morphology. Since flexoelectricity depends on a strain gradient rather than homogenous strain, it has an advantage in that it is not restricted to non-centrosymmetric crystal morphologies. Since strain gradients can create polarization in any material, they have more applications than homogenous strain. However, creating large strain gradients can be difficult and can cause mechanical failure. Since only small strain gradients can be achieved in bulk materials, their flexoelectric effect is unnoticeable. Therefore, 2D materials offer a great platform for creating large strain gradients and producing flexoelectric effects, while also avoiding causing damage to the material. This is one of the reasons why this research chooses to use WS₂ in its study of electromechanical coupling.

2.2 Flexoelectricity

This section will provide a description of flexoelectricity and the strategies used to measure it in WS₂. First, the direct and converse flexoelectric effects and the advantages of measuring flexoelectricity in WS₂, a transition metal dichalcogenide, are discussed. Then the method by which piezorespone force microscopy measures flexoelectricity, and Kogan's estimate, a formula for estimating the flexoelectric response, are examined. Finally, a brief summary synthesizes the key points in this chapter and outlines what to expect from the experiments.

2.2.1 Direct and Converse Effect

Similarly to piezoelectricity, flexoelectricity also displays both a direct and converse effect. For the direct effect, an applied strain gradient creates a polarization and for the converse effect, an applied electric field creates stress. The formulas for the two equations are shown below.

$$P_i = \mu_{ijkl} \frac{\partial \varepsilon_{jk}}{\partial x_l}$$

$$\sigma_{ij} = \mu_{ijkl}^* \frac{\partial E_k}{\partial x_l}$$

P , E , μ , ε , σ , represent polarization, electric field, the flexoelectric coefficient, strain, and stress, respectively. The subscripts i, j, k, and l represent the cartesian directions.

Putting the formulas for electromechanical coupling together, the resultant equations are shown below.

$$P_i = d_{ijk} \sigma_{jk} + \mu_{ijkl} \frac{\partial \varepsilon_{jk}}{\partial x_l}$$

$$\sigma_{ij} = e_{ijk} E_i + \mu_{ijkl} \frac{\partial E_k}{\partial x_l}$$

In both equations, the first term is due to the piezoelectric effect and the second term is due to the flexoelectric effect. Here e is the piezoelectric tensor, but is dependent on stress instead of strain. One can see that piezoelectricity and flexoelectricity both contribute to the effects of electromechanical cou-

pling. Therefore, it may be difficult to isolate flexoelectricity from piezoelectricity during experimentation. However, transition metal dichalcogenides, including WS₂, offer a convenient way to single out flexoelectric behavior.

2.2.2 Why Monolayer WS₂?

Previous work demonstrates the existence of flexoelectricity in monolayer MoS₂ and its corresponding coefficient[11]. In this work, since single layer MoS₂ yields no piezoelectric response to perpendicular strain or a perpendicular electric field, but does have an out-of-plane flexoelectric response, any electromechanical response discovered would be due to flexoelectricity [12]. The piezoelectric tensor for TMDs below shows why there is no out-of-plane piezoelectric response [11].

$$d_{ij} = \begin{bmatrix} d_{11} & -d_{11} & 0 & 0 & 0 & 0 \\ 0 & 0 & 0 & 0 & 0 & -2d_{11} \\ 0 & 0 & 0 & 0 & 0 & 0 \end{bmatrix}$$

The indices correspond to the formula for converse piezoelectricity, repeated below.

$$\varepsilon_j = d_{ij} E_i$$

Therefore, since the piezoelectric tensor only has in-plane coefficients, there should be no out-of-plane piezoelectric effect when a perpendicular electric field is applied. On the other hand, the flexoelectric tensor for TMDs

is shown below. This tensor uses Voigt notation to convert four indices into two indices.

$$\mu_{ij} = \begin{bmatrix} \mu_{11} & 0 & 0 & 0 & \mu_{15} & 0 & 0 & 0 & \mu_{19} \\ \mu_{11} & 0 & 0 & 0 & \mu_{15} & 0 & 0 & 0 & \mu_{19} \\ \mu_{31} & 0 & 0 & 0 & \mu_{31} & 0 & 0 & 0 & \mu_{39} \\ 0 & 0 & 0 & 0 & 0 & \mu_{46} & 0 & \mu_{48} & 0 \\ 0 & 0 & \mu_{46} & 0 & 0 & 0 & \mu_{48} & 0 & 0 \\ 0 & \mu_{11} - \mu_{15} & 0 & \mu_{11} - \mu_{15} & 0 & 0 & 0 & 0 & 0 \end{bmatrix}$$

The indices correspond to the formula for converse flexoelectricity, repeated below.

$$\sigma_{ij} = \mu_{ijkl} \frac{\partial E_k}{\partial x_l}$$

Here, the first six columns of the matrix can be eliminated, since the applied electric field will be perpendicular to the surface of the material. Additionally, the first two rows can be eliminated, because they correspond to the in-plane stress created, which will not be measured. Therefore, the nonzero coefficients μ_{48} and μ_{39} will constitute the out-of-plane electromechanical response.

For this experiment, monolayer material is investigated. 2D materials offer a great platform for the study of flexoelectricity due to their small size. Additionally, the number of applications for 2D materials in nanodevices is

growing and studying electromechanical coupling in 2D materials will allow for innovation in these technologies. For the TMDs, materials with an odd number of layers (1, 3, ...) have been shown to demonstrate in-plane piezoelectricity in literature[11]. Therefore monolayer WS₂ demonstrates electromechanical properties and is a good subject to further the understanding of flexoelectricity, and how it operates as a form of electromechanical coupling.

By taking advantage of the fact that TMDs have no out-of-plane piezoelectric effect, the research mentioned above applied an electric field perpendicular to the surface of MoS₂, and the converse flexoelectric effect was measured. Since WS₂, also a transition metal dichalcogenide, has the same crystal structure as MoS₂, D_{3h} ($\bar{6}m2$), the same morphological implications apply[13]. For WS₂, a similar experiment can be performed to further the understanding of flexoelectricity. By applying an electric field perpendicular to the surface of WS₂, the corresponding flexoelectricity can be measured. To measure this converse effect, piezoresponse force microscopy is used.

2.2.3 Piezoresponse Force Microscopy

Piezoresponse force microscopy (PFM) measures the out-of-plane electromechanical deformation that occurs when an electric field is applied to the surface of WS₂. The conductive tip of an atomic force microscope is used to apply an electric field perpendicular to the surface of a material. Then the corresponding contracting and relaxing caused by the electromechanical

response is recorded by the displacement of the tip. In this fashion, since monolayer WS₂ has no out-of-plane piezoelectric activity, the converse flexoelectric effect can be measured. A more detailed description of the mechanics of PFM is provided in Chapter 3 and the results of the PFM measurements are shown in Chapter 4.

One of the parameters of the PFM experiment is the drive voltage. This is the voltage at the conductive tip that is used to create the electric field perpendicular to the material. In the experiment, the drive voltage is varied to see if there is a difference in the flexoelectric coefficient derived from the measurements. Since the flexoelectric coefficient is an intrinsic property of the material, it should not change over a voltage sweep. Consistency in the coefficients calculated would corroborate the findings of the experiment.

2.2.4 Kogan's Estimate

Before performing any measurements, it is useful to first develop an estimate of the expected flexoelectric response. This estimate can be used later to understand the results of the experiment. Kogan's estimate is used to get an order of magnitude estimate of the expected flexoelectric coefficient[14]. The equations are presented below.

$$f \approx \frac{q}{4\pi\epsilon_0 a}$$

$$\mu \approx \chi f$$

Here a , the lattice constant, is 3.19 \AA [13] and χ , susceptibility, is 3.13 [15] for WS_2 . Therefore, we get a 0.125 nC/m for μ , the flexoelectric coefficient. If the experimental value recorded in this research is on the order of this estimation, the estimation would play a corroborative role in this thesis.

2.2.5 Summary

In conclusion, piezoelectricity represents the relationship between homogenous strain and polarization, and flexoelectricity represents the relationship between strain gradients and polarization. However, each electromechanical coupling effect can manifest in both direct and converse effects, and piezoelectricity and flexoelectricity may be difficult to separate from each other. To solve this problem, this work takes advantage of that fact that the crystal class for TMDs has no out-of-plane piezoelectric effect, but does have an out-of-plane flexoelectric effect. Therefore, out-of-plane flexoelectricity in WS_2 can be viably measured, knowing that out-of-plane piezoelectricity is absent. Piezoresponse force microscopy is used to apply a perpendicular electric field and measure the converse flexoelectric effect of WS_2 . Finally, the value reached by experimentation should be on the order of 0.125 nC/m .

Chapter 3

Methods

3.1 Sample Preparation

Sample preparation can be divided into two key steps: cleaning the substrate and exfoliation. In this project, gold-coated silicon is used as the substrate and the sample was exfoliated using the tape method.

3.1.1 Cleaning the Substrate

For these experiments, gold-coated silicon was used as the substrate due to its high electrical conductivity, which is necessary for PFM measurements. Specifically, gold is used to help confine the electric field within the WS₂ and acts as the bottom electrode. Since this project focuses primarily on using monolayer material, which is less than a nanometer in height, it is important that the surface of the substrate is as clean as possible. Small,

unwanted particles on the surface of the gold could easily interfere with the PFM measurements. Therefore, cleaning the substrate is an integral part of preparing the samples.

The cleaning process uses a sonicator extensively. A sonicator is a machine that uses sound energy to dislodge adsorbed particles from a sample surface via mechanical vibration. In our experiments, the sonicator was used to remove contaminants. First, a sonicator is filled with deionized (DI) water. Then, acetone is placed in a beaker in the sonicator. The gold substrate is inserted in the beaker and sonicated for five minutes. After that, the same process is repeated twice, except the beaker is filled with isopropyl alcohol (IPA) and then DI water instead. The water droplets left on the surface are removed with a nitrogen gun. At last, organic surface contaminants are removed using O₂ plasma cleaning. These steps help ensure that the substrate is as clean as possible before WS₂ is exfoliated and transferred onto the surface of the gold substrate.

3.1.2 Mechanical Exfoliation

First, flakes of WS₂ were placed onto blue polyethylene cleanroom tape and repeatedly thinned by pressing both sticky sides together. Repeatedly thinning the WS₂ increases the chances of finding monolayer material, but also creates smaller areas of interest since the pieces of WS₂ are torn apart. Therefore, through trial and error, it was found that approximately ten cycles of folding open and folding closed the tape was optimal for finding sizable

monolayer areas. After that, the WS₂ on the tape was exfoliated onto polydimethylsiloxane (PDMS). The PDMS was then examined under with an optical microscope to see if there were areas which could contain monolayer material. Finally, the WS₂ on the PDMS was transferred onto the gold-coated substrate by exfoliation. Figure 3.1 and 3.2 show this process. After this the sample is ready for the next step: finding monolayer areas.



(a) Place a piece of WS₂ onto the tape.

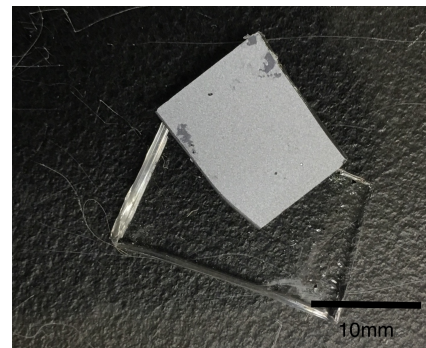


(b) Repeatedly fold open and fold close the tape for exfoliation.

Figure 3.1: Mechanical Exfoliation of WS₂



(a) Transfer the WS₂ from the tape to the PDMS.



(b) Transfer the WS₂ from the PDMS to the gold.

Figure 3.2: Transfer of WS₂ onto Gold

3.2 Characterizing Monolayer WS₂

Once a sample has been prepared, it is necessary to identify a monolayer area for eventual characterization by PFM. First, the sample is examined under an optical microscope to find thin layers, which appear nearly transparent and are almost the same color as the gold. Next, these thin layers are examined with Raman spectroscopy, photoluminescence, and atomic force microscopy, to see if they consist of a single atomic layers, i.e., monolayers. This next section will give an overview of these three processes and describe how they help identify monolayer material.

3.2.1 Raman Spectroscopy

Raman spectroscopy is used in this study to determine the number of layers of WS₂ for a given area of interest. Raman spectroscopy is a commonly used method to determine a material's composition. First, the material is illuminated with a laser at a selected wavelength. Most of this light scatters through an elastic process, where energy is conserved; however, some of it scatters inelastically by creating or absorbing mechanical vibrations in the material (Raman effect). The shift in energy for the inelastically scattered light is measured to obtain the energy of the scattered vibrational mode. For the purpose of this experiment, this method is used to help identify monolayer WS₂ regions since the energies of the vibrational modes can depend on the thickness of the material. In this experiment, a 532 nm wavelength laser was

used and through the Raman scattering process, the vibrational modes of the system were revealed. These act as signatures for the different number of layers in a WS_2 sample.

Published results of the Raman spectra for WS_2 under 532 nanometer wavelength laser illumination are shown below [16] in Figure 3.3. This figure shows that as the number of layers decreases, the out-of-plane A_{1g} peak decreases in magnitude. Additionally, the peak at 310 cm^{-1} disappears for monolayer material. Although the author of this text admits the origin of this mode is unclear, a similar peak is also found in monolayer WSe_2 . For our experiments, the disappearance of the 310 cm^{-1} peak will be used as a benchmark to determine whether or not the area of interest contains monolayer material.

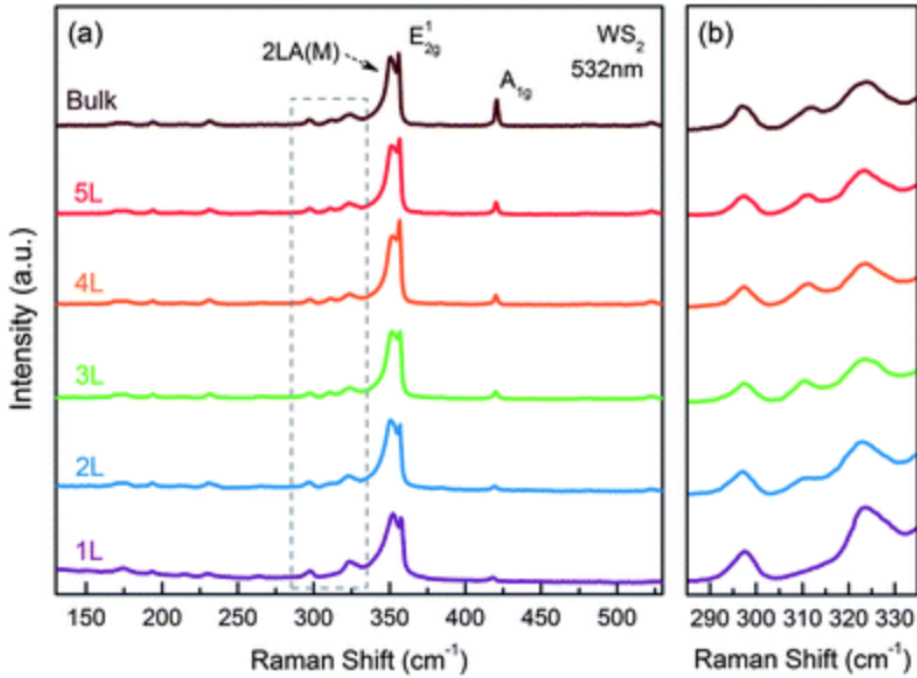


Figure 3.3: (a) The Raman spectra of WS₂ under a 532 nm wavelength light demonstrating the decreasing A_{1g} mode. (b) Section of the spectra demonstrating the disappearing mode at 310 cm⁻¹. The figure shows Raman plots for the different number of layers and labels the Raman modes (e.g. A_{1g}, E_{2g}¹, 2LA(M)). [16]

3.2.2 Photoluminescence

Similarly to Raman spectroscopy, photoluminescence (PL) was performed using a 532 nm wavelength laser illumination to help determine the number of layers of WS₂. PL works by shining a light, or photons, onto a material (photoexcitation), and measuring the distribution in energy of the photons that are re-radiated. PL is especially useful for differentiating direct-gap

and indirect-gap materials, since direct-gap materials exhibit much stronger radiative recombination than indirect-gap materials. More simply stated, direct-gap materials emit light more quickly and with much greater intensity. Since monolayer WS₂ is direct gap and bulk WS₂ is indirect-gap, monolayer WS₂ will have a stronger PL signal than bulk WS₂ [17]. This characteristic is used in combination with Raman spectroscopy to help identify monolayer WS₂.

3.3 Atomic Force Microscopy

Atomic force microscopy (AFM) is used in conjunction with Raman spectroscopy and photoluminescence to help identify monolayer WS₂. AFM can provide many different types of information, but for this research, it was mainly used for height information. Height information acts as another indication of layer number, because height values for WS₂ are well-known and widely cited in papers[17]. Additionally, AFM measures the topography of the material so that it is easy to identify different features.

An AFM has a cantilever with a small probe, more commonly called the “tip,” at the end. Figure 3.4 shows a schematic illustration of an AFM probe tip, sample, and apparatus for detecting motion of the tip. [18]. In this instrument, a laser shines on the back of the cantilever and reflects onto a photodiode. Deflection of the cantilever causes a displacement of the laser beam on the photodiode and the variations in position of the laser on the

photodiode are measured to determine the motion of the tip.

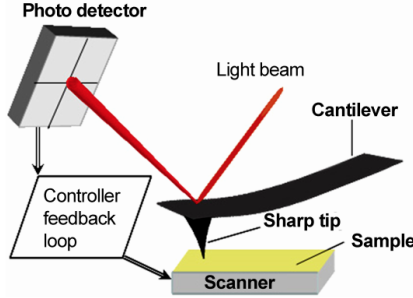


Figure 3.4: AFM measurement system showing cantilever, tip, light beam, and photo detector.[18]

To determine the topography of the sample surface, the AFM tip scans in a raster pattern on the surface of the material. The height of the tip is measured allowing the surface topography to be determined at a resolution limited by the tip size. AFM has three imaging modes: contact, tapping, and non-contact. In non-contact mode, the tip never touches the surface, and therefore yields a lower resolution. For this thesis, contact and tapping mode were used. Contact mode was used for cleaning the surface and tapping mode was used for high-resolution height measurements. Contact mode works by dragging the tip across the surface of the material. Although contact mode does record useful information, tapping-mode was used for data collection since it produces less wear on the tip and has a smaller chance of altering the material. Contact mode was used to clean the surface of WS₂, because it moves small contaminant particles to the edges of the scan window and helps clean the area of interest. Tapping mode operates by having the cantilever

oscillate above the surface at its resonance frequency, a factory-determined value, during a scan. This oscillation allows for the tip to come close to the surface with only intermittent contact, resulting in much less damage to the tip compared to dragging the tip in contact mode. Changes in the amplitude of this oscillation are detected by a lock-in amplifier. The lock-in amplifier takes the signal from the deflection of the photodiode and isolates the selected frequency component. This datum is then used to create the height image. In this manner, tapping mode can be used to record height information.

While studying WS₂, the primary use of AFM was recording height information. AFM height images are useful for determining the number of layers of WS₂, and examples of height images will be presented and discussed in the Chapter 4. Important parameters that are chosen by the user and purposefully recorded during both contact and tapping mode are: scan dimensions, scan rate, tip velocity, samples/line, number of lines, integral gain, proportional gain, and amplitude or deflection setpoint, depending on the measurement taken. The samples/line and number of lines parameters determines the resolution of the image. The integral gain and proportional gain parameters help calibrate the feedback for the system, which keeps the deflection of the tip at a constant level. Additionally, tapping mode has an amplitude setpoint value, the distance of the tip apex from the surface. A high amplitude setpoint means the tip is high off the surface and interacting less with the material. This means that the user wants to protect the

tip, but yields a less precise measurement of the surface. A lower amplitude setpoint means the tip is closer to the surface and the user is willing to risk the integrity of the tip for higher precision. Contact mode does not have an amplitude setpoint since the tip rests on the surface continuously. However, it does have its own deflection setpoint. This deflection setpoint controls the deflection of the cantilever. The higher the deflection setpoint, the further the tip is tilted onto the surface of the material. If the deflection has a relatively high value, the image will be clearer, but this also risks damaging the tip. If the deflection has a relatively low value, the tip is protected, but the image may be less clear. These parameters all give useful information about the environment and conditions under which the image was taken.

3.4 Piezoresponse Force Microscopy

Once a monolayer area of WS₂ has been identified, piezoresponse force microscopy (PFM) can be used to measure the electromechanical response for WS₂. The largest part of this project focused on taking PFM measurements and analyzing the data. PFM is a version of the contact mode AFM measurement with a conductive tip [19]. A drive voltage oscillating with a drive frequency is applied to the tip. This creates an electric field perpendicular to the surface of the tip. The sample is placed on a conductive coin, which is connected to ground. The tip is typically scanned in a raster pattern on the surface of the material, similarly to AFM. However, since the tip is

conductive, an electric field is applied to the material. For flexoelectric materials, an out-of-plane electromechanical response will be present, causing the material to move and the cantilever to deflect. The cantilever deflection is measured by the laser deflection on the photodiode. The data from the photodiode is then sent to the lock-in amplifier which selects the information that is at the drive frequency. This ensures that the information collected is due to the applied voltage and not other factors that are present. Finally, the output of the PFM is represented by amplitude and phase values. The amplitude corresponds to the magnitude of the signal and the phase to the phase difference from the original drive signal, at the drive frequency.

When performing PFM measurements, specific parameters are selected and must be recorded for later data analysis. Similarly to AFM measurements, scan size, aspect ratio, scan rate, tip velocity, samples/line, number of lines, integral gain, and proportional gain should be recorded. Also, since PFM is a version of contact mode AFM, the deflection setpoint should be recorded. Additionally, the drive amplitude and deflection sensitivity should be recorded. The drive amplitude and deflection sensitivity are especially important as they are integral to quantifying the electromechanical response. The drive amplitude is the magnitude of the voltage that is applied across the material to create the electric field. This is selected during the experiment setup. The deflection sensitivity is a calibration value used to find the amount of mechanical motion caused by the applied voltage. Specifically, the deflection sensitivity is used to convert the recorded voltage value

into a displacement value. The two values of the PFM output, amplitude and phase, are measurements of voltage and time delay, respectively, but a displacement value is needed to understand the electromechanical effects of PFM. The amplitude and phase values can be thought of as a vector with a voltage magnitude equal to the value of its amplitude. This voltage value can then be converted to a physical displacement value. The deflection sensitivity, with units of nm/V is used to perform this conversion. The calibration process is done right before any PFM measurement. First the cantilever is placed onto the surface of the material and a Z-piezo tube slowly extends the cantilever down, causing the cantilever to bend. This deflection over time is measured by the photodiode. The Z-piezo tube moves the cantilever down by a predetermined, factory setting value. The factory calculated value and the slope of the deflection of the photodiode are compared to determine the deflection sensitivity. Once the deflection sensitivity is set, the voltage output of the PFM measurement can be converted into a displacement.

With the drive amplitude, deflection sensitivity, amplitude, and phase recorded, enough data has been recorded for the calculation of electromechanical response. The data analysis will be presented in the experimental results section.

Chapter 4

Experimental Results

4.1 Characterizing Monolayer WS₂

After preparing a sample of WS₂ and looking for thin material regions under an optical microscope, multiple areas that looked transparent were found. However, after Raman spectroscopy and photoluminescence (PL) measurements only one of these areas contained material that was found to be monolayer. Figure 4.1 shows an optical image of the area of interest. The first arrow points to the monolayer area and the second arrow points to multilayer, possibly bilayer, WS₂. To determine layer thickness, first Raman spectroscopy was performed.

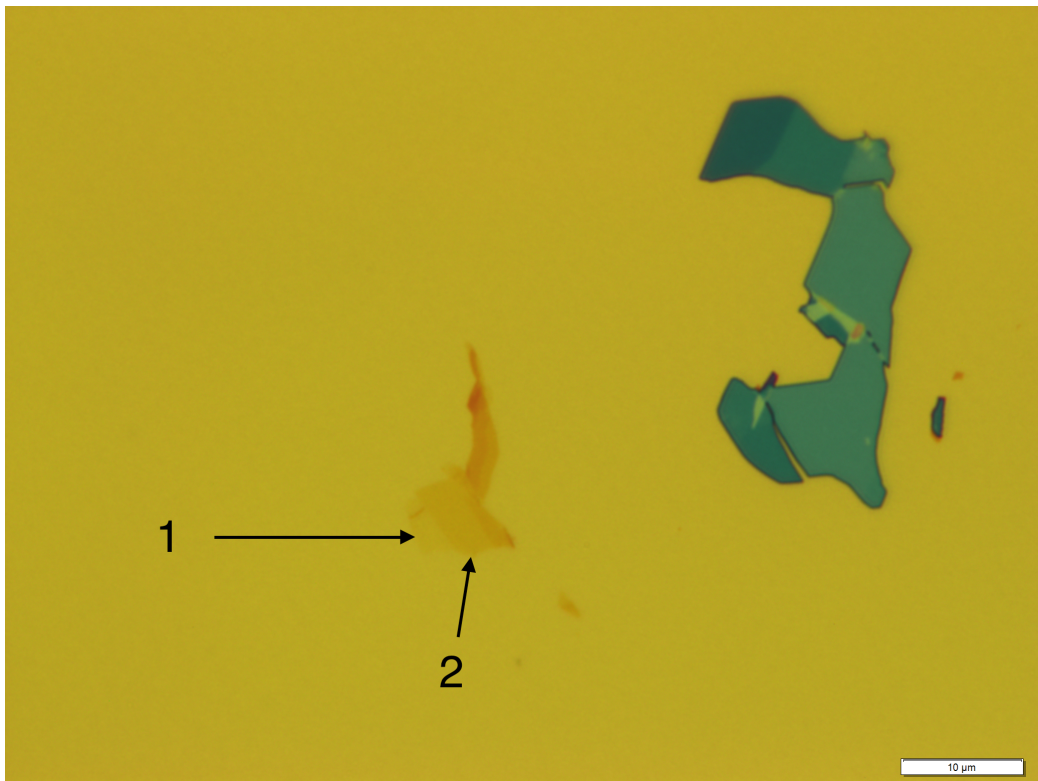


Figure 4.1: An optical image of WS₂. The (1) points to a monolayer region and the (2) points to multilayer, possibly bilayer, region.

4.1.1 Raman Spectroscopy

The Raman spectra at two points in the area of interest were used to determine the existence of monolayer WS₂. The first point is on the suspected monolayer area and the second is on the suspected multilayer area to the right of it. These areas are depicted in Figure 4.1. A graph of the Raman spectra for both areas is shown in Figure 4.2. One can see that the signal for the multilayer area is much stronger than the signal for the monolayer area.

This can be attributed to the presence of more material in multilayer regions, which gives the incoming photons more to interact with and therefore creates more inelastic scattering. Additionally, one can conclude that the area on the left in Figure 4.2 contains fewer layers since the A_{1g} mode produced on the area on the left is smaller than that produced on the right. Nevertheless, this does not confirm the region on the left is a monolayer region. Figure 4.3 depicts an enlarged spectrum centering around 310 cm^{-1} . As discussed in the previous chapter, the monolayer area should be missing a peak at 310 cm^{-1} that exists in the multilayer material; however, it is very hard to see if this is actually the case. After multiple trials, at different laser excitation intensities and lengths, the results were the same. Unlike MoSe_2 and WSe_2 , which are also transition metal dichalcogenides that have, respectively, disappearing B_{2g} and an interlayer shear modes for monolayer material, WS_2 has no easily recognizable Raman features[20]. Although, the absence of a Raman peak at 310 cm^{-1} for WS_2 is discussed in literature, its absence was not recognizable in the experiments performed [16]. This could be attributed to the existence of any peak at 310 cm^{-1} being lower than the noise floor of the measurement system, or the fact that this experiment uses a different substrate than the literature - gold instead of silicon dioxide [16]. However, since monolayer WS_2 is a direct band gap material, this study can rely on photoluminescence to prove the existence of monolayer WS_2 .

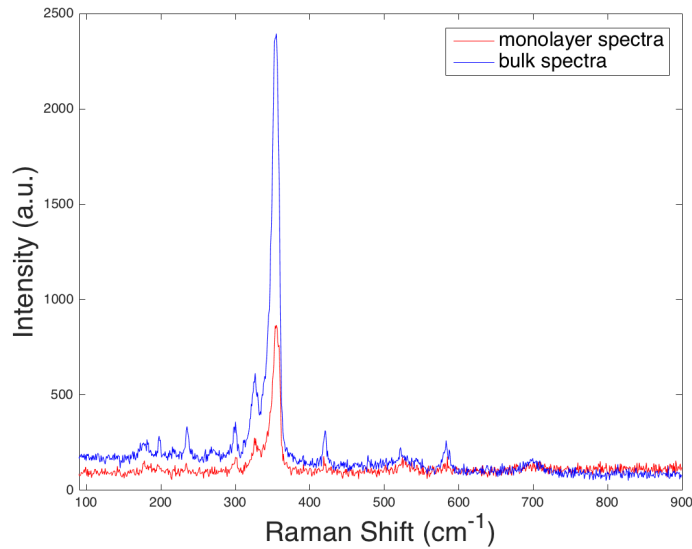


Figure 4.2: Raman spectra of monolayer and multilayer WS_2 .

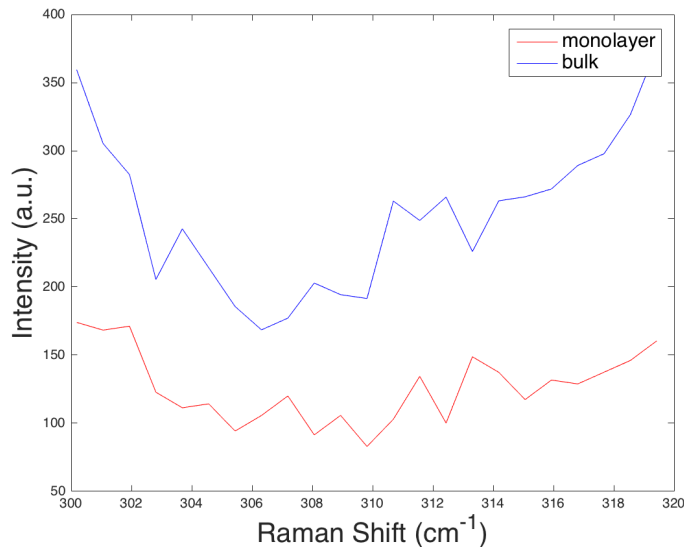


Figure 4.3: Enlarged view of Raman spectra of WS_2 . Here we can see that the presence of a peak at 310 cm^{-1} in the multilayer material cannot be definitely determined.

4.1.2 Photoluminescence

The photoluminescence spectra at two points on the area of interest, shown on Figure 4.1, were used to look for monolayer material. As discussed in the previous chapter, since monolayer WS₂ is a direct band gap material it will luminesce much more efficiently and intensely than multilayer material. This can be seen below in Figure 4.4. These signatures match the literature and therefore, provide more definitive evidence that monolayer material has been found [17].

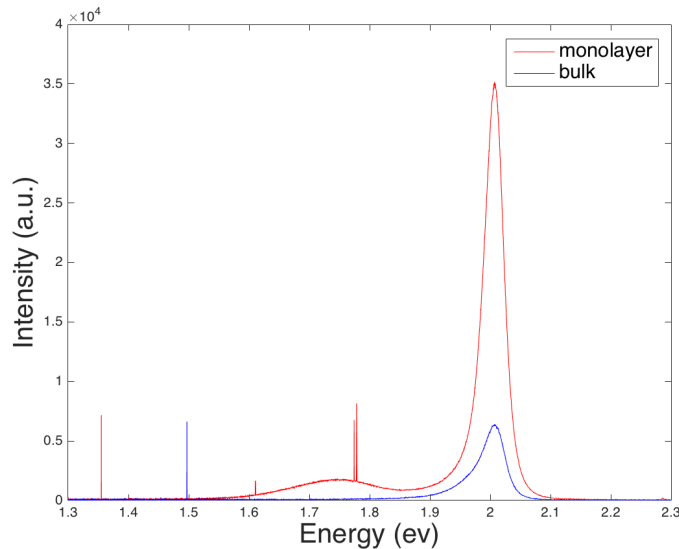
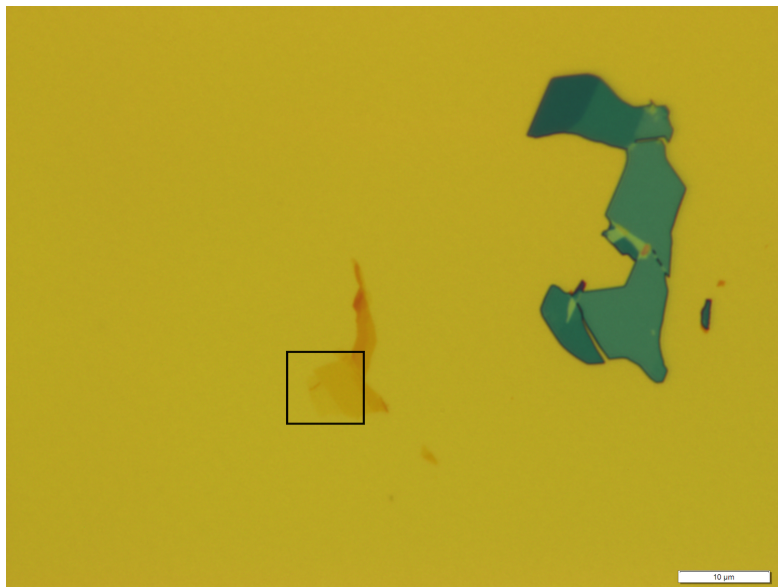


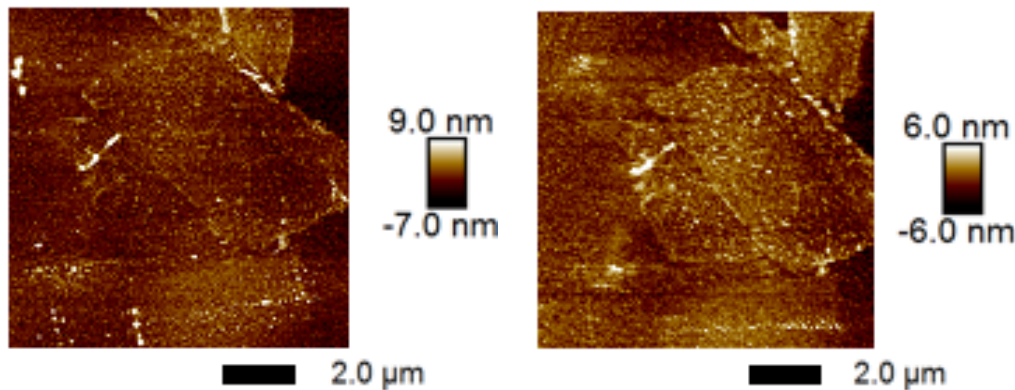
Figure 4.4: Photoluminescence spectra for monolayer (red line) and bulk (blue line) WS₂. Monolayer WS₂ can be identified due to the much greater intensity of the luminescence peak at 2.0 eV, a consequence of the direct band gap of monolayer WS₂ and indirect band gap of bulk WS₂. The skinny peaks throughout the graph are due to noise in the system.

4.2 Atomic Force Microscopy

To further support the conclusion drawn in the previous section, the relative heights of the material will be discussed. Tapping mode AFM was performed to characterize the topography of the material. However after capturing a height image, it was evident the material had many surface contaminants. Contact mode AFM was performed to clean the material surface using the process discussed in the previous chapter. Then, tapping mode AFM was again performed to get a topographic image. Figure 4.5 shows which part of the area of interest was selected for the height analysis, and tapping mode images before and after the contact mode cleaning procedure. It is evident that some contaminants, corresponding to peaks in the topography, were pushed to the side during the contact mode experiment. The tapping mode image can be read as the thickness of the material, which acts as another indicator of the number of layers. In a paper using SiO_2 as the substrate for WS_2 , the height difference between the SiO_2 and WS_2 was found to be 1 nm and the height difference between the first layer of WS_2 and the second to be 0.6 nm[17]. 0.6 nm represent the “true” thickness of monolayer WS_2 and the larger difference between the substrate and first layer of WS_2 is due to tip-sample and sample-substrate interactions and is well documented in literature[17].



(a) Original optical image with area selected for tapping mode AFM indicated by the black rectangle. The scale bar is 10 micrometers.

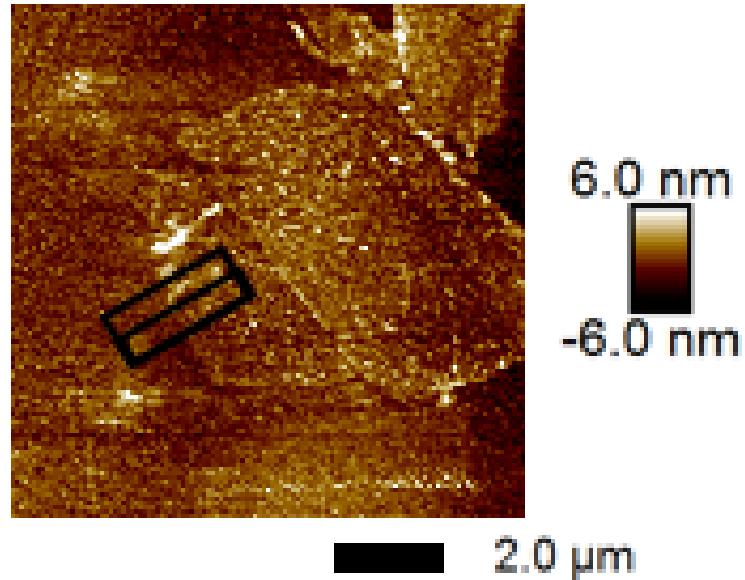


(b) Original topographic image before contact mode cleaning. (c) Topographic image after contact mode cleaning.

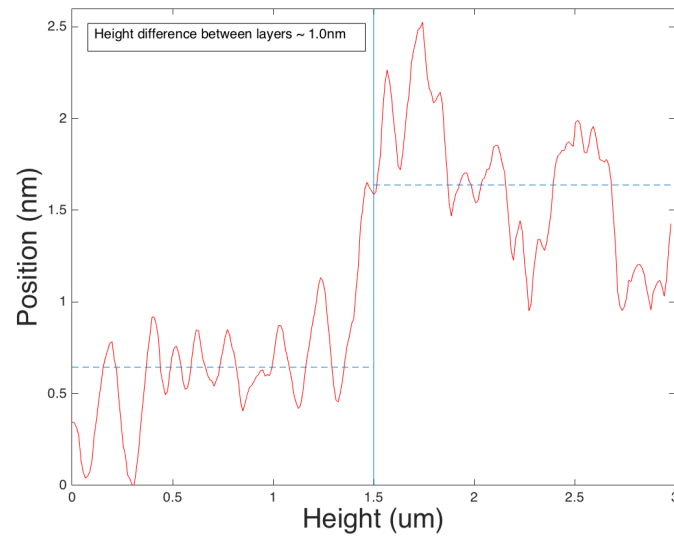
Figure 4.5: WS₂ area selected (a), Tapping mode image before contact mode cleaning (b), and Tapping mode image after contact mode cleaning (c)

In the measurements performed in this experiment similar results were found. To find the height difference between gold and the first layer of WS₂,

and the height difference between the first and second layer of WS_2 , a rotated rectangular section of the material was exported out of the NanoScope Analysis software. The Nanoscope Analysis software takes vertical averages across a horizontal(lengthwise) sweep to find the height average of each vertical slice. Figure 4.6(a) shows the cross section over the substrate and thinner WS_2 . Figure 4.6(b) shows the height average of each vertical slice for this cross section. To find the step height from the substrate to the monolayer, the average height of each area was calculated. Then the difference between the two averages was calculated to find the distance between the two layers. The average height from the gold to the first layer of WS_2 was 1.0 nm. Figure 4.7(a) shows the cross section over the first layer of WS_2 and the multilayer WS_2 . Figure 4.6(b) shows the height average of each vertical slice for this cross section. The average distance was calculated with the same method and found to be 0.65 nm. These values are very similar to the results from literature and add to the evidence that monolayer material exists in the area of interest. Additionally, one can surmise that the multilayer area is bilayer material, although given the Raman spectra and photoluminescence data limitations, it is hard to argue that the region is bilayer with certainty.

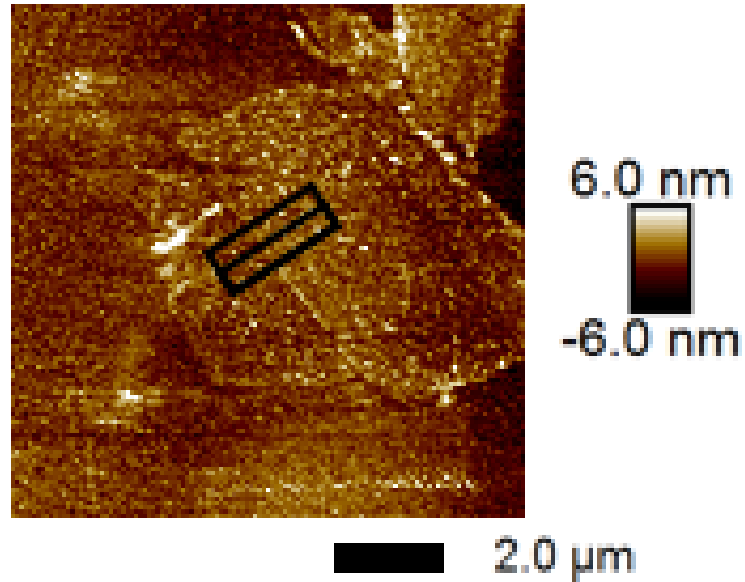


(a) Topographic image of WS_2 with the cross section of gold and the first layer of WS_2 indicated by the black rectangle. The color scale shows relative heights with lighter regions being higher than darker regions.

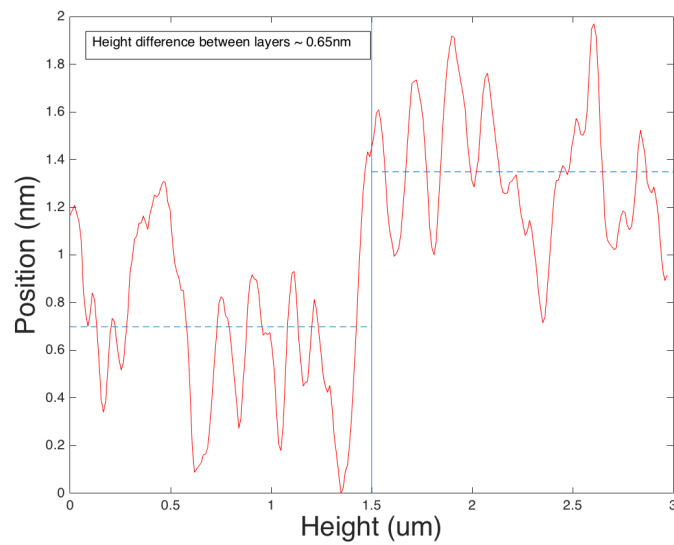


(b) Vertical height averages over the cross section. Gold is on the left and monolayer WS_2 is on the right.

Figure 4.6: Height difference between gold and the first layer of WS_2



(a) Topographic image of WS₂ with the cross section of the first and second layer of WS₂ indicated by the black rectangle. The color scale shows relative heights with lighter regions being higher than darker regions.



(b) Vertical height averages over the cross section. Monolayer WS₂ is on the left and bilayer WS₂ is on the right.

Figure 4.7: Height difference between the first and second layer of WS₂

4.3 Piezoresponse Force Microscopy

Once the presence of monolayer WS₂ has been confirmed, PFM is performed to determine the effective piezoelectric coefficient. The area selected for PFM is shown in Figure 4.8 and includes both monolayer and gold area for three important reasons. First, it is necessary to see contrast in the response between the gold and monolayer regions that would exist due to flexoelectric behavior. Second, both areas are needed to apply the background subtraction method that is discussed later in this chapter. Finally, it is useful to have both sample and substrate areas during one PFM scan since tip wear and other uncontrolled environment variables can change between experiments.

For this experiment, PFM was performed at different drive voltages to see if changing the drive voltage affected the determination of the effective piezoelectric coefficient d_{33}^{eff} . As discussed in Chapter 2, d_{33}^{eff} is not expected to change under different drive voltages. Figure 4.9 shows the data under different drive voltages. The outputs of PFM are an amplitude and phase signal. These signals will later be used during the background subtraction section to calculate the piezoelectric constant. As expected, 0 V applied to the material shows no contrast between the gold and monolayer WS₂. As the voltage increases, one can see that the contrast is more pronounced. The effective piezoelectric coefficient will be calculated for all of these trials, excluding 0 volts.

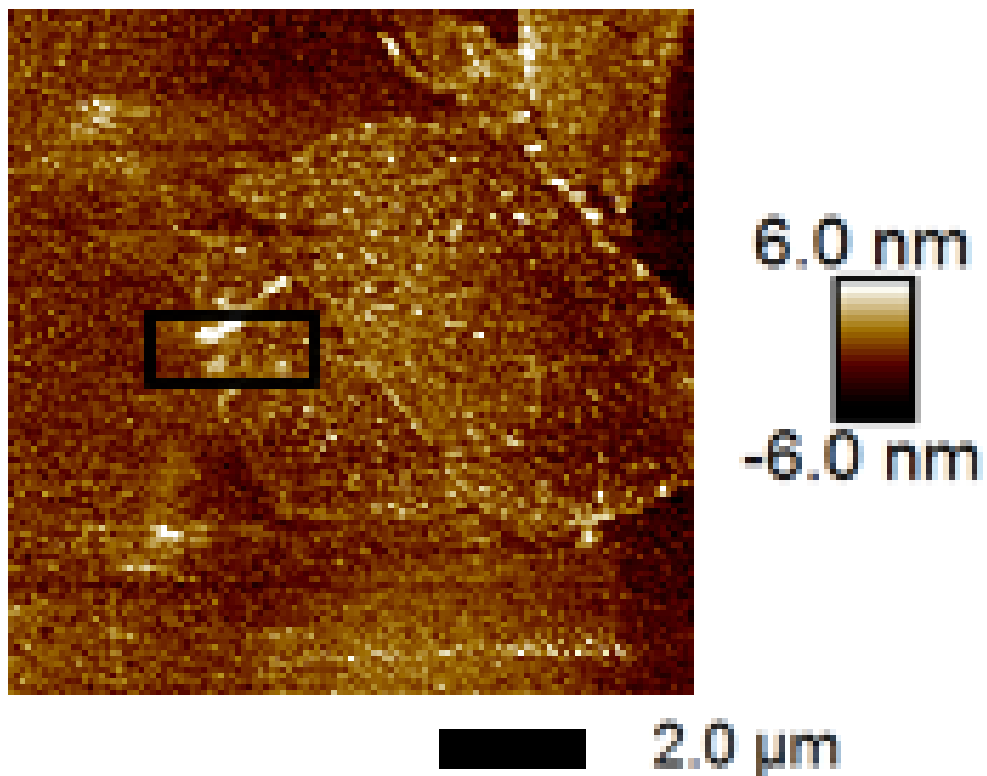


Figure 4.8: Area selected for PFM characterization of WS₂.

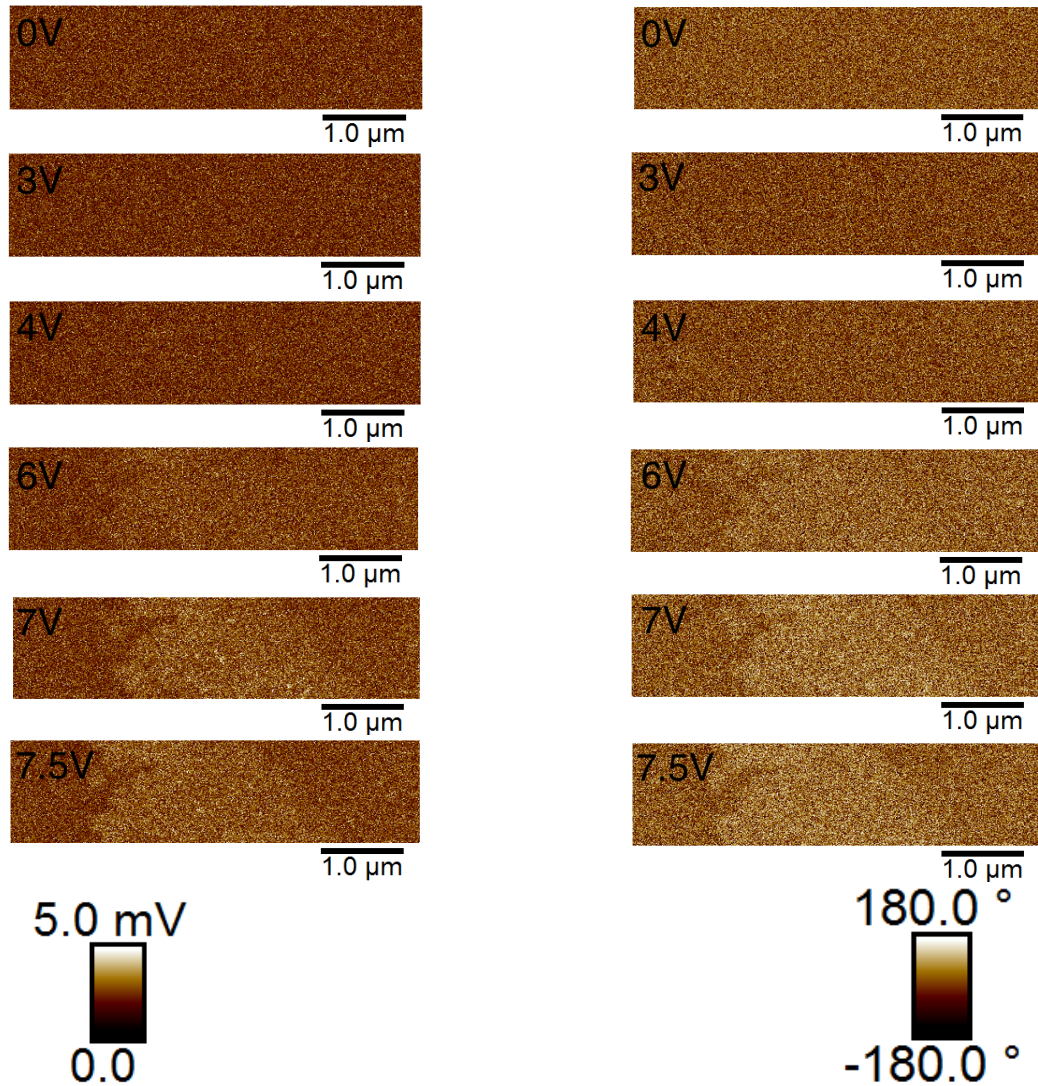


Figure 4.9: PFM Measurements of WS_2

4.4 Background Subtraction Method

Reliable and accurate PFM measurements require careful selection of parameters, thorough analysis, and awareness of the potential of artifacts[21]. In particular, frequency dependence, artifacts of the feedback system, thermal noise, and other system-specific behaviors must be recognized and accounted for. Although frequency dependence should not occur if the drive frequency differs from the contact-resonant frequency, the experiment shows that this is not the case. To help deal with the above issues, a background subtraction technique from literature will be used to analyze the PFM data [21]. Since PFM yields amplitude and phase signals, those values can be converted into x- and y-components to generate a vector. Once these vectors have been generated, vector subtraction can be used to remove the background contributions. Removing the substrate vector allows us to understand the behavior of the monolayer material. Figure 4.10 shows a visual example of this subtraction. Once vector subtraction has been performed, the new x-component and y-component can be recombined to find the adjusted PFM magnitude which will be used in the final analysis. This adjusted value represents the signal without contributions from the substrate or measurement system.

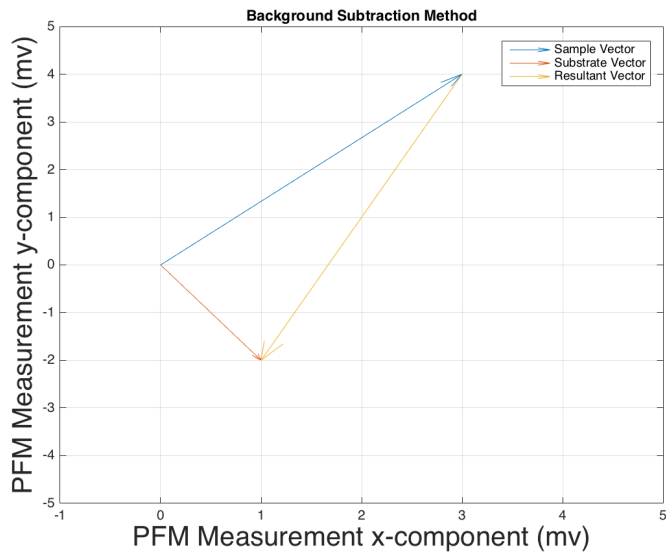


Figure 4.10: Background Subtraction Method

4.5 Calculating d_{33}^{eff}

Finally, to calculate the piezoelectric constant d_{33}^{eff} , the equation below is used.

$$d_{33}^{\text{eff}} = \frac{(\text{Adjusted PFM signal}) * (\text{Deflection Sensitivity})}{(\text{Drive Voltage} * \text{Gain})}$$

First, areas of both substrate and sample are selected. These selected areas are kept constant for both amplitude and phase and for each PFM trial. The selected area is depicted in Figure 4.11 on one of the amplitude scans.

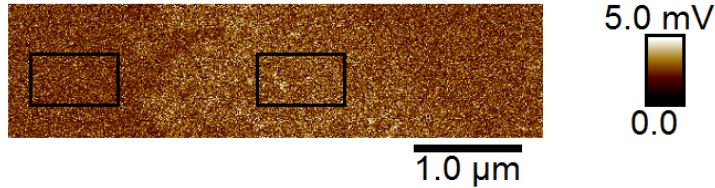


Figure 4.11: Selected area for data analysis. The area on the left is gold and the area on the right is monolayer WS_2 .

Each area is averaged for both their amplitude and phase values. Then, the background subtraction method is performed on these averaged values to obtain the *AdjustedPFMsignal*. The *deflection sensitivity* is the calibrated value that translates the voltage output of the PFM into a displacement value. A more detailed explanation of the deflection sensitivity is provided in Chapter 3. For this experiment, the calibrated value was 80.5 nm/V. The *Drive Voltage* is the voltage applied during the different trials and the *Gain* is a hardware gain factor. The *Drive Voltage* values have been adjusted, because when measuring the actual voltage applied to the system with an oscilloscope, the voltages were slightly lower than expected. A table of drive voltage adjustments has been provided below. The d_{33}^{eff} has been calculated for each drive voltage and the results are provided in the next section.

Applied Voltage	Measured Voltage
0.00	0.000
3.00	2.950
4.00	3.906
5.00	4.875
7.00	6.780
7.50	7.250

Table 4.1: Table 1. Voltages selected in the PFM software vs. voltages actually applied during the measurement.

4.6 Summary of Results

Figure 4.12 below shows the results of the experiment. One key feature to notice is that, unlike discussed in Chapter 2, the d_{33}^{eff} is not the same for different drive voltages. This feature and possible reasons why it exists will be discussed in the next chapter. Additionally, an extra measurement at 6.78V was provided to show variation at the same drive voltage.

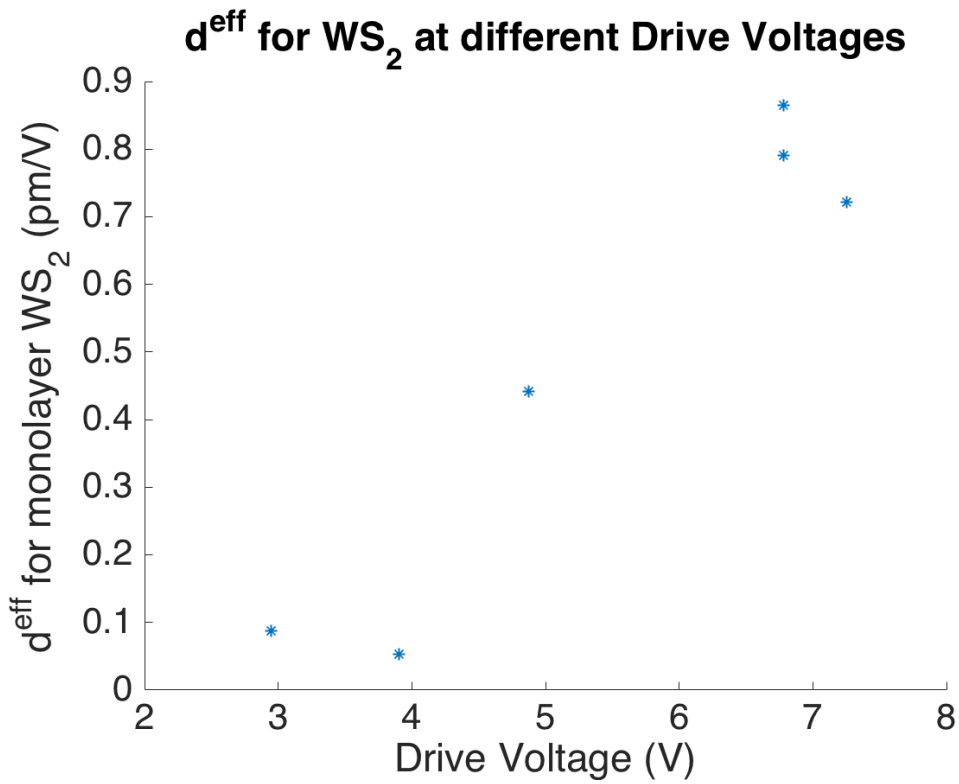


Figure 4.12: Results

Chapter 5

Conclusion

5.1 Understanding the Results and Limitations of the Experiment

The d^{eff} at different drive voltages presented in the previous chapter is reproduced in Figure 5.1. As explained in Chapter 2, since flexoelectricity is a property intrinsic to a given material, the d^{eff} should not vary over a voltage sweep. However, as the results show, the measured value seems to vary, especially for the two lower points measured at 2.90V and 3.91V drive voltage. One possible reason for the reduced measured value at low voltages is material clamping. Since the electric field applied by the PFM tip is localized around the tip, material not directly below or around the tip will demonstrate limited electromechanical coupling. These areas will suppress the electromechanical response of the areas below the tip and therefore reduce

the response[22]. This effect is called material clamping. At low voltages, material clamping may drastically reduce electromechanical response and therefore, effect out-of-plane measurements.

Additionally, PFM has some unavoidable contributions to the measurements[22]. As discussed before, some of these contributions are taken into account and subtracted out using a background subtraction method from literature. However, there are other factors in play that are not accounted for by the background subtraction method. For example, a given PFM tip may experience wear and tear during the experiment that may affect the voltage applied as well as the displacement measured. To reduce these effects, the measurements provided in this thesis were all taken during the same experiment and with the same tip. However, any changes in the tip over the duration of the experiment may have an effect on the data collected. Therefore, material clamping and PFM measurement particulars may explain variation in the measured electromechanical response.

The average value for d^{eff} is calculated to be 0.66 ± 0.18 pm/V where the uncertainty value is the standard deviation over multiple experiments. Removing the points affected by material clamping, the d^{eff} is calculated to be 0.79 ± 0.07 pm/V. This value, when compared to that of MoS₂, fits the trend predicted by Kogan's estimate[11]. The calculation of μ^{eff} and a comparison to Kogan's estimate is discussed next.

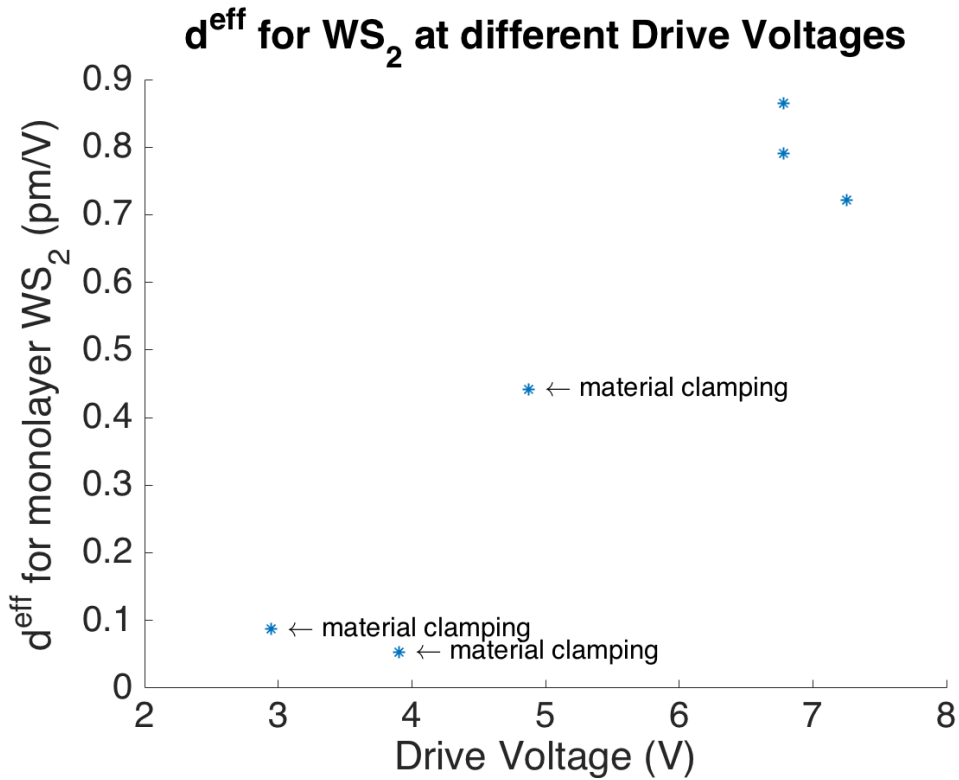


Figure 5.1: Results annotated with expected material clamping for low voltages.

5.2 Comparison to Kogan's Estimate

In Chapter 2, Kogan's estimate for the flexoelectric coefficient, μ , for WS₂ was calculated to be 0.125 nC/m. To see if the measurements performed in the experiment are reasonably close to Kogan's estimate, first we must calculate μ^{eff} . To calculate the μ^{eff} from the vertical deflection measured by PFM, d^{eff} , the equations below are used.

$$\varepsilon = \frac{\Delta z}{t}$$

Here, ε , Δz , and t are strain, measured vertical deflection, and thickness, respectively. Combining this equation with the formula for converse piezoelectricity (from Chapter 2), the equation below relates d^{eff} with the measured vertical deflection.

$$d^{\text{eff}} = \frac{\Delta z}{tE}$$

Next, the two equations below are combined with the equation for converse flexoelectricity (from Chapter 2) to finally relate μ^{eff} to d^{eff} .

$$\sigma = Y\varepsilon$$

$$\frac{\partial E}{\partial x} \approx \frac{2V}{t^2}$$

Here, σ , Y , E , and V are stress, Young's modulus, the electric field and drive voltage, respectively. The second equation is an estimation for the electric field used in literature[11]. Finally, an equation relating μ^{eff} to d^{eff} is presented below.

$$\mu^{\text{eff}} = d^{\text{eff}} \cdot Y \cdot \frac{t}{2}$$

The value for Young's modulus is taken from literature [1]. Using the

equation above, the μ^{eff} is calculated to be 0.050 nC/m. Since Kogan's estimate provides an order of magnitude approximation, the value calculated in Chapter 2 provides corroboration to the results of the experiment.

5.3 Summary of Research and Future Work

The research in this thesis demonstrates progress in the understanding of electromechanical effects in TMDs, specifically WS₂. Since an out-of-plane electromechanical response in TMD materials cannot be attributed to piezoelectricity, this measured response acts as evidence for flexoelectricity. Additionally, this thesis shows that 2D materials are a good platform for studying flexoelectricity and it provides an avenue for comparing flexoelectric theory with experiment. Finally, the demonstration of an out-of-plane polarization allows for an increase in the applications of piezoelectric properties, such as energy harvesters, sensors, and actuators. Overall, this thesis helps develop an understanding of flexoelectricity, characterizes electromechanical effects in WS₂, and demonstrates potential applications in 2D materials.

As previously mentioned, the apparent dependence of the d^{eff} for WS₂ on the drive voltage was unexpected. Taking more PFM measurements on several samples of monolayer WS₂ will help better characterize this behavior. Additionally, Jungk et al. describes a method for reducing material clamping and this could be implemented in future experiments[22]. Future work could also consider the flexoelectric behavior of other TMDs. In our lab, PFM ex-

periments on WS₂ happened in conjunction with experiments on two other TMDs, MoSe₂ and WSe₂. Each of these four matched the trend predicted by Kogan’s estimate, except WSe₂. Future work would investigate possible reasons why WSe₂ does not match this trend. Another experiment could take advantage of the fact that TMDs are composed of monolayers. Since TMDs can be split into single layers and stacked, heterostructures combining two layers of TMDs can be created[23]. In this scenario, the out-of-plane effect would theoretically be enhanced since crystal symmetry would be further broken. Measuring flexoelectricity in these materials would provide interesting results and help characterize the electromechanical effect.

Biography

Kalhan Koul is an undergraduate student in Electrical and Computer Engineering Honors and Plan II Honors at The University of Texas at Austin. In engineering, Kalhan's interests are in computer architecture and digital design. During his time at UT Austin, Kalhan was part of a entrepreneurship team that created a device that detected driver drowsiness. During his summers, he completed internships at Texas Instruments and Silicon Labs. Additionally, Kalhan has been involved in student societies such as Plan Tutoring, Roden Leadership program, and Eta Kappa Nu (Honors Electrical Engineering). Kalhan is a Distinguished College Scholar in Engineering and Liberal Arts, a recipient of the Virgina and Ernest Cockrell, Jr. Scholarship, and a recipient of the Unrestricted Endowed Presidential Scholarship. After finishing his undergraduate degree, Kalhan plans on pursuing a PhD in Computer Engineering.

Bibliography

1. Duerloo, K.-A. N., Ong, M. T. & Reed, E. J. Intrinsic Piezoelectricity in Two-Dimensional Materials. *Physical Chemistry* **19**, 2871–2876 (2012).
2. Akinwande, D. *et al.* A review on mechanics and mechanical properties of 2D materials - Graphene and beyond. *Science Direct* **13**, 42–77 (2017).
3. Zubko, P., Catalan, G. & Tagantsev, A. K. Flexoelectric Effect in Solids. *Annual Review of Materials Research* **43**, 387–421 (2013).
4. Maranganti, R., Sharma, N. D. & Sharma, P. Electromechanical coupling in nonpiezoelectric materials due to nanoscale nonlocal size effects: Green's function solutions and embedded inclusions. *APS* **74**, 014110 (2006).
5. He, L. *et al.* On the coupling effects of piezoelectricity and flexoelectricity in piezoelectric nanostructures. *AIP Advances* **7**, 105106 (2017).
6. Maranganti, R., Sharma, N. D. & Sharma, P. Electromechanical coupling in nonpiezoelectric materials due to nanoscale nonlocal size effects:

- Green's function solutions and embedded inclusions. *Physical Review B* **74**, 014110 (2006).
7. Wang, Z. L. The new field of nanopiezotronics. *Science Direct* **10**, 20–28 (2007).
 8. Hill, E. W., Vijayaraghavan, A. & Novoselov, K. Graphene Sensors. *IEEE Sensors Journal* **11**, 12 (2011).
 9. Wang, Q.-M., Du, X.-H., Xu, B. & Cross, L. E. Electromechanical Coupling and Output Efficiency of Piezoelectric Bending Actuators. *IEEE Transactions on Ultrasonics, Ferroelectrics, and Frequency control* **46**, 3 (1999).
 10. Erhart, J. Experiments to demonstrate piezoelectric and pyroelectric effects. *Physics Education* **48**, 438 (2013).
 11. Brennan, C. J. *et al.* Out-of-Plane Electromechanical Response of Monolayer Molybdenum Disulfide Measured by Piezoresponse Force Microscopy. *Nano Letters* **17**, 5464–5471 (2017).
 12. Shu, L., Wei, X., Pang, T., Yao, X. & Wang, C. Symmetry of flexoelectric coefficients in crystalline medium. *Applied Physics* **110**, 104106 (2011).
 13. Duerloo, K.-A. N., Ong, M. T. & Reed, E. J. Intrinsic Piezoelectricity in Two-Dimensional Materials. *Physical Chemistry Letters* **3**, 2871?2876 (2012).

14. Kogan, S. M. Piezoelectric Effect During Inhomogenous Deformation and Acoustic Scattering of Carriers in Crystals. *Soviet Physics - Solid State* **5**, 10 (1964).
15. Ramasubramaniam, A. Large excitonic effects in monolayers of molybdenum and tungsten dichalcogenides. *Physical Review* **86**, 115409 (2012).
16. Zhao, W. *et al.* Lattice dynamics in mono- and few-layer sheets of WS₂ and WSe₂. *Nanoscale* **5**, 9677–9683 (2013).
17. Gutierrez, H. R. *et al.* Extraordinary Room-Temperature Photoluminescence in Triangular WS₂ Monolayers. *Nano Letters* **21**, 3447–3454 (2013).
18. Pletikapic, G. & DeNardis, N. I. Application of surface analytical methods for hazardous situation in the Adriatic Sea: monitoring of organic matter dynamics and oil pollution. *Natural Hazards and Earth Science Systems* **17**, 31–44 (2017).
19. Soergel, E. Piezoresponse force microscopy (PFM). *Applied Physics* **44**, 464003 (2011).
20. Tonndorf, P. *et al.* Photoluminescence emission and Raman response of monolayer MoS₂, MoSe₂, and WSe₂. *The Optical Society* **21**, 4908–4916 (2013).
21. Jungk, T., Hoffmann, A. & Soergel, E. Quantitative analysis of ferroelectric domain imaging with piezoresponse force microscopy. *Applied Physics Letters* **89**, 163507 (2006).

22. Jungk, T., Hoffmann, A. & Soergel, E. Challenges for the determination of piezoelectric constants with piezoresponse force microscopy. *Applied Physics Letters* **91**, 253511 (2007).
23. Li, M.-Y., Chen, C.-H., Shi, Y. & Li, L.-J. Heterostructures based on two-dimensional layered materials and their potential applications. *Materials Today* **19**, 6 (2016).